Nanoscale

PAPER

View Article Online
View Journal | View Issue



Cite this: *Nanoscale*, 2016, **8**, 13695

# Size dependent electrochemical detection of trace heavy metal ions based on nano-patterned carbon sphere electrodes†

Lu-Hua Zhang, Wen-Cui Li, Dong Yan, Hua Wang and An-Hui Lu*

Received 18th May 2016,
Accepted 21st June 2016

DOI: 10.1039/c6nr04019e

www.rsc.org/nanoscale

The challenge in efficient electrochemical detection of trace heavy metal ions (HMI) for early warning is to construct an electrode with a nano-patterned architecture. In this study, a range of carbon electrodes with ordered structures were fabricated using colloidal hollow carbon nanospheres (HCSs) as sensing materials for trace HMI (represented by Pb(II)) detection by square wave anodic stripping voltammetry. The regular geometrical characteristics of the carbon electrode allow it to act as a model system for the estimation of electron transfer pathways by calculating contact points between HCSs and a glassy carbon electrode. A clear correlation between the contact points and the electron transfer resistance has been established, which fits well with the quadratic function model and is dependent on the size of HCSs. To our knowledge, this is the first clear function that expresses the structure–sensing activity relationship of carbon-based electrodes. The prepared carbon electrode is capable of sensing Pb(II) with a sensitivity of 0.160 μA $nM^{-1}$, which is much higher than those of other electrodes reported in the literature. Its detection limit of 0.6 nM is far below the guideline value (72 nM) given by the US Environmental Protection Agency. In addition, the carbon electrode could be a robust alternative to various heavy metal sensors.

## Introduction

In consideration of the growing water pollution by heavy metal ions (HMI) and its great threat to human health, developing sensing strategies for HMI detection for early warning is urgently needed.[1] Among various existing techniques, the electrochemical method, *i.e.*, square wave anodic stripping voltammetry (SWASV), has attracted significant attention due to its portability of devices and short analysis time.[2] To satisfy the custom-tailored requirements of competitive sensitivity and low detection limit for trace amounts of HMI, it is mandatory to fabricate electrodes with a rapid collection capacity of HMI and fast electron transport along the electron pathway.[3–5] Following this line, a variety of nanostructured porous carbonaceous materials, *e.g.*, zero-dimensional nanoparticles,[6–8] one-dimensional carbon nanotubes,[9,10] and two-dimensional graphene nanosheets,[11–14] have been used as sensing materials to modify electrodes for stripping analysis of HMI due to their large specific surface area and high conductivity. However, most of the promising electrodes could not achieve a satisfactory sensing performance. In most cases, the electrodes were constructed from randomly distributed material units so that only statistical results were obtained. Thus, a fundamental understanding of the actual structure–activity relationship of the electrodes is limited, consequently holding up the innovation of electrode materials.

The structural disorder at the contact between two nanoparticles always leads to unwanted enhancement in the scattering of free electrons, thus reducing efficient electron mobility, consequently hindering progress in achieving high efficiency.[15,16] On the contrary, an ordered and interconnected electrode architecture makes them attractive electron percolation pathways for vectorial electron transfer between interfaces.[17,18] In the fields of dye-sensitized solar cells, researchers have also found that an ordered electrode possessed excellent light-to-electricity conversion efficiency in comparison to the disordered one. Therefore, we believed, for the detection of trace amounts of Pb(II) using SWASV, the ingenuity that goes into an ordered electrode architecture may be capable of improving vectorial electron transport from an electrode to an electrolyte, rather than simply improving the electro-activity of sensing materials.

Apparently, at the current stage the key is to explore new electrode materials which can act as model systems for understanding the correlation between the electrode structure and sensing performance. Under this consideration, spherical

*State Key Laboratory of Fine Chemicals, School of Chemical Engineering, Dalian University of Technology, Dalian 116024, P. R. China. E-mail: anhuilu@dlut.edu.cn; Fax: +86 411-84986112; Tel: +86 411-84986112*

†Electronic supplementary information (ESI) available. See DOI: 10.1039/c6nr04019e

carbon colloids would be a satisfactory sensing material due to their ability to assemble into a well-ordered structure, offering the potential for improved electron percolation transport for vectorial charge transfer between interfaces. The regular geometrical characteristics of an electrode model make it possible to correlate the sensing performance with the structure.[19] Meanwhile, carbon nanospheres have high surface area and good electro-conductivity, showing high adsorption capacity for heavy metal ions and fast electron transfer rates. However, the self-assembly of carbon spheres has to be precisely controlled. A successful assembly of long-range ordered crystalline layers requires exquisite control over many parameters, such as solvent dispersibility, sphere size distribution, solvent evaporation kinetics, and so on.[20–22]

In this study, a range of carbon electrodes with well-organized structures were fabricated using colloidal hollow carbon nanospheres (HCSs) as sensing materials. Specifically, the successful preparation of HCSs[23,24] with perfect spherical shape, tunable but uniform diameters, and solvent dispersible properties are the prerequisite for the self-assembled patterned structure formation. Consequently, the regular geometrical characteristics of the carbon electrode allow it to act as a model system for the estimation of electron transfer pathways by calculating the contact points between HCSs and a glassy carbon electrode (GCE), building a bridge between the electrode architecture and sensing performance. With the increased contact points, the current signal increased and the optimum value is achieved when the contact points reach up to $7.62 \times 10^8$. Electrochemical impedance spectroscopy was used to understand the superior efficiency of the carbon electrode. We have found a clear correlation between the contact points and electron transfer resistance ($R_{et}$), which fits well with the quadratic function model. In other words, the optimum current signal corresponds to the smallest $R_{et}$. To our knowledge, this is the first clear function that expresses the structure–sensing activity relationship of carbon-based electrodes. The prepared carbon electrode is capable of sensing Pb(II) with a sensitivity of 0.160 μA $nM^{-1}$, which is much higher than those of other electrodes reported in the literature. Its detection limit of 0.6 nM is far below the guideline value (72 nM) given by the US Environmental Protection Agency (EPA). In addition, the carbon electrode could be a robust alternative to various heavy metal sensors.

## Results and discussion

Assembling HCSs into well-ordered structures on the surface of GCE was accomplished by solvent evaporation induced aggregating assembly at the air–liquid interface. The obtained HCSs were firstly dispersed in an ethanol solution. As shown in Fig. S1a,† the dispersed solution of the HCSs is very stable, with no sign of aggregated precipitation over 3 days. The polydispersity index (PDI) of these HCSs in ethanol solution is approximately 0.026 (Fig. S1b†), thus indicating discrete and highly dispersible HCSs and the uniformity in the sizes. This suspension was then pipetted onto the surface of a freshly polished GCE. After the evaporation of ethanol (approximately minutes), a carbon film was stably supported on the GCE surface. The scanning electron microscopy (SEM) images in Fig. 1a and S2† show that HCSs have assembled into close-packed crystal layers over large areas. Consequently, the carbon electrode with a well-organized structure has predictable electron pathways by calculating the contact points between the HCSs and GCE by a single layer close packing sphere model (Fig. 1b and Part II in the ESI†). When the fabricated carbon electrode is used for the electrochemical detection of trace Pb(II) in an aqueous solution using SWASV, a stripping peak can be obtained, as illustrated in Fig. 1c.

It is obvious that the amounts of electron pathways of the carbon electrodes can be easily changed by employing HCSs with different sizes, bridging between the electrode architecture and sensing performance. With the intention of exploring the structure–sensing activity relationship of the carbon electrode, HCSs with different internal void sizes and similar shell thicknesses were synthesized by choosing polystyrene (PS) nanosphere templates with different diameters. As shown in Fig. 2a and b, the carbon shell thicknesses are about 33 ± 2 nm and internal void sizes of two HCS samples are 265 ± 4 nm and 188 ± 3 nm, which are denoted as HCS-265-33 and HCS-188-33 respectively (HCS-*x*-*y*, *x* and *y* represent the sizes of internal void and shell thickness respectively). For a given sample, about 50 HCSs were quantified to obtain the average values of the void and shell thickness. As expected, the obtained HCSs are discrete, dispersible, and uniform. The prepared HCSs with similar pore structures and amorphous features,[23] which thus minimize the influence of other variable factors, provide a suitable model to investigate the relevance of the electrode structure and sensing performance. Fig. 2c shows the SWASV response of HCS-188-33 and HCS-265-33 modified GCEs in the presence of 0.25 μM Pb(II) in 0.1 M NaAc–HAc solution. It illustrates that Pb(II) was detected at a

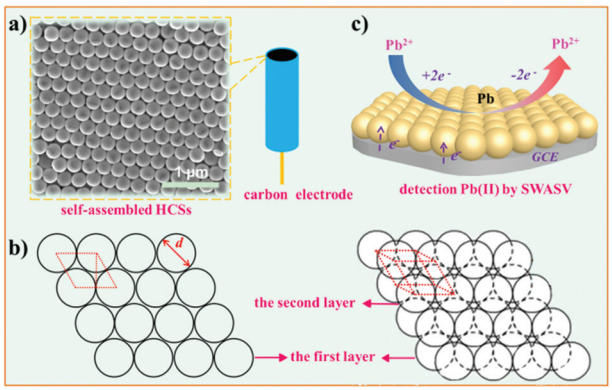


Fig. 1 (a) SEM image of the self-assembled HCS-188-44. (b) The scheme of the first layer (left) and ordered structures (right) of the hexagonal close-packed structure model. As shown, the area of the element is $0.866d^2$. The volume and void of the element is $0.707d^3$ and $0.183d^3$, respectively. The void fraction is 0.259. (c) The process of the electrochemical detection of trace Pb(II) in an aqueous solution using SWASV.

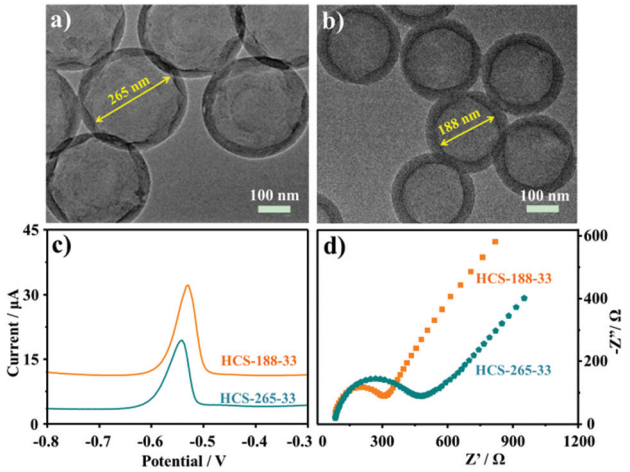


**Fig. 2** TEM images of the carbon samples: (a) HCS-265-33 and (b) HCS-188-33. (c) SWASV response (background current was subtracted) of HCS-188-33 and HCS-265-33 modified electrodes in the presence of 0.25 μM Pb(II) in 0.1 M NaAc–HAc solution (pH = 5.5). (d) Nyquist plots of HCS-188-33 and HCS-265-33 modified electrodes in the solution of 5 mM $Fe(CN)_6^{3-/4-}$ and 0.1 M KCl.

potential of approximately −0.55 V with well-defined peaks. Remarkably, the stripping peak current of HCS-188-33 (21.1 μA) is higher than that of HCS-265-33 (15.8 μA) (Table 1).

To attain a clear understanding of the sensing performance, an impedance study was carried out to determine the feasibility of electron transfer on different electrode surfaces. All electrochemical measurements were performed in a solution containing 5 mM $Fe(CN)_6^{3-/4-}$ and 0.1 M KCl. The Nyquist plot shows that the two electrodes have a semicircular region followed by a straight line (Fig. 2d). The semicircle portion, observed at higher frequencies, corresponds to the electron-transfer-limited process. The semicircle diameter equals the electron transfer resistance ($R_{et}$). At the lower frequencies, a straight sloping line represents diffusive resistance (Warburg impendence ($Z_w$)).[25–27] Thus, the results were fitted into a general electronic equivalent circuit of an electrochemical cell (Randles model). The fitting of one measured curve to the equivalent circuit (solid line) is shown in Fig. S3,† indicating good agreement with the circuit model (dotted line) and the measurement system over the entire measurement frequency range. The $R_{et}$ value corresponding to HCS-188-33 is about 199.0 Ω, which is nearly a half smaller than that of HCS-265-33 (340.3 Ω), implying the increased electron transfer from the electrode to the electrolyte (Table 1).[5,26,27]

For a given mass and shell thickness of the HCSs, the smaller the void diameter of HCS is, the larger the number of HCSs spread on the GCE, thus more contact points between HCSs and GCE, consequently, increased electron transfer pathways from the electrode to the electrolyte (Fig. S4†). The contact points between the HCSs and GCE are calculated by a single layer close packing model. As shown in Table 1, the estimated contact points between the HCS-188-33 and GCE are $8.99 \times 10^8$, while $5.29 \times 10^8$ for HCS-265-33. The difference between HCS-188-33 and HCS-265-33 is $3.70 \times 10^8$. At the same time, with the decrease of the size of the void, the spheres become tightly packed, resulting in the formation of a continuous conductive network to enhance the electron transfer. These may be the two primary causes of the resultant low $R_{ct}$ of HCS-188-33.

Based on the effect of the void size of HCSs on the sensing performance, HCSs with different shell thicknesses and similar sizes of voids were prepared to modify GCEs in order to figure out the influence of shell thickness on the activity of the electrode. By altering the molar ratio of the phenol and formaldehyde (PF) precursor to the PS template, HCSs with different shell thicknesses and similar internal void sizes were obtained. Fig. 2b and 3a–c are the TEM images of HCS-188-33, HCS-188-44, HCS-188-55 and HCS-188-79 samples. The void sizes of the four HCS samples are all 188 ± 3 nm and the shell thicknesses are accordingly 33 ± 2, 44 ± 2, 55 ± 2, and 79 ± 2 nm. After a polynomial fitting, a good function of shell thickness *vs.* precursor phenol concentration can be established (Fig. 3d and Table S1†). This enables one to alter the coating

**Table 1** Structure parameters and sensing performance of the carbon electrodes

| Electrode | Current signal (μA) | $R_{et}$ (Ω) | $D_{HCS}$ [a] (nm) | $n$ [b] |
|---|---|---|---|---|
| HCS-265-33 | 15.8 | 340.3 | 331 | $5.29 \times 10^8$ |
| HCS-188-33 | 21.1 | 199.0 | 254 | $8.99 \times 10^8$ |
| HCS-188-44 | 40.7 | 72.3 | 276 | $7.62 \times 10^8$ |
| HCS-188-55 | 29.4 | 121.0 | 298 | $6.53 \times 10^8$ |
| HCS-188-79 | 11.8 | 498.6 | 346 | $4.84 \times 10^8$ |

[a] $D_{HCS}$: the diameter of HCSs. For a given sample, about 50 HCSs were quantified to obtain the average value of diameter. [b] $n$: the number of contact points between HCSs and GCE.

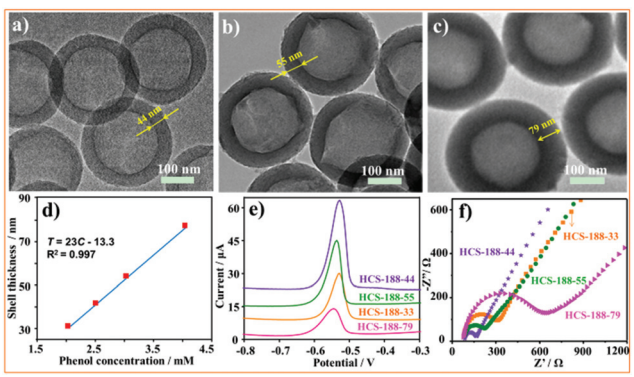


**Fig. 3** TEM images of the carbon spheres: (a) HCS-188-44, (b) HCS-188-55, and (c) HCS-188-79 samples. (d) Using a PS template with the diameter of 200 nm, the correlation between the phenol concentration ($C$) and the carbon shell thickness ($T$) of HCSs. (e) SWASV response of HCS-188-33, HCS-188-44, HCS-188-55 and HCS-188-79 modified electrodes in the presence of 0.25 μM Pb(II) in 0.1 M NaAc–HAc solution (pH = 5.5). (f) Nyquist plots of HCS-188-33, HCS-188-44, HCS-188-55 and HCS-188-79 modified electrodes in the solution of 5 mM $Fe(CN)_6^{3-/4-}$ and 0.1 M KCl.

thickness continuously over a wide range of 33–79 nm by simply changing the mass ratio of the reactants, confirming the precise control of the carbon shell at the nanoscale. The surface areas and pore structures of all the HCS samples were investigated using $N_2$ adsorption techniques. As shown in Fig. S5 and Table S1,† the nitrogen adsorption isotherms of all the samples are essentially pseudo-type II, showing interparticle capillary condensation. The surface area and pore volume of all the samples are similar. Besides, the precursor, polymerization and pyrolysis temperature are the same. All in all, the prepared HCS samples with similar surface areas, pore structures and surface chemical properties, which thus minimize the influence of other variable factors, provide a suitable model to investigate the relevance of the electrode structure and sensing performance.

As listed in Table 1, with the decrease in the thickness of the carbon shell from 79 nm to 33 nm, the contact points between the HCSs and GCE increase from $4.84 \times 10^8$ to $8.99 \times 10^8$. A successive increase in the contact points decreases the $R_{et}$ to 72.3 Ω, with an improved current signal. The optimum current signal of 40.7 μA is observed, when the contact points reach up to $7.62 \times 10^8$ (Fig. 3e and f). With more increased contact points from $7.62 \times 10^8$ to $8.99 \times 10^8$, the current signal strongly decreased to 21.1 μA. The $R_{et}$ value also significantly increased from 72.3 Ω to 199.0 Ω. This may be attributed to the increased resistance at HCSs–HCSs and HCSs–GCE interfaces of the carbon electrode with more increased contact points, which leads to a poor charge transportation and further sensing performance.[26] Thus, there exists a "golden size" for the HCSs, with which an electrochemical system has a minimum electron-transfer resistance.

Interestingly, when we fit the relation of $R_{et}$ and contact points ($n$), a good quadratic function of $R_{et}$ *vs.* $n$ is obtained (red curve), with a high correlation coefficient of 0.980 (Fig. 4). To the best of our knowledge, this is the first time that a clear function is established to express the structure–sensing activity relationship of carbon-based electrodes, indicating that the sensing activity is virtually dependent on the sizes of HCSs. It is worth noting that the discovery of a "golden size" of HCSs is attributed to the nano-patterned structure of HCSs on the surface of the GCE. Further, the highly discrete and dispersible

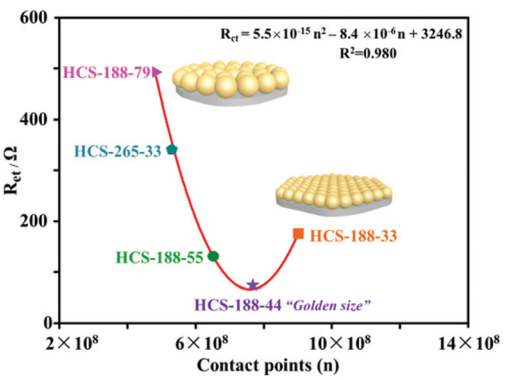


Fig. 4 $R_{et}$ as a function of contact points ($n$).

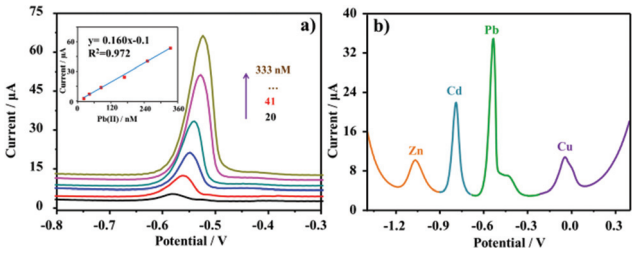


Fig. 5 (a) SWASV response of a HCS-188-44 modified GCE for analysis of Pb(II) over a concentration range of 20 to 333 nm. Inset: Calibration plots of the current signal *vs.* the concentration of Pb(II). (b) Simultaneous analysis of 83 nM Zn(II), Cd(II), Pb(II) and Cu(II) in 0.1 M NaAc–HAc solution.

HCSs with high uniformity are the determinants in the formation of the self-assembled patterned structure.

Hence, the electrochemical sensing performance of HCS-188-44 was studied further in detail. Fig. 5a shows the SWASV response towards aqueous Pb(II) solutions with different concentrations, and the corresponding calibration curves are derived accordingly (Fig. 5a inset). As shown, the stripping peak current is proportional to the concentration of Pb(II) from 20 to 333 nM. The linearization equation is $y = 0.160 \times -0.1$, with the correlation coefficients of 0.972. As a result, the sensitivity is as high as 0.160 μA $nmol^{-1}$, which is much higher than those of other electrodes reported in the literature (see Table 2). Therefore, the application of a microstructure-controlled electrode in the detection of Pb(II) is an effective way to push performance limits forward. The detection limit of the carbon electrode is calculated to be 0.6 nM (3δ method), which is significantly lower than the guideline value of 72 nM in drinking water given by the US EPA.

In addition to Pb(II) detection, we attempt to investigate the sensing performance of the HCS-188-44 toward the detection of several metal ions simultaneously. The SWASV response for simultaneous analysis of Zn(II), Cd(II), Pb(II), and Cu(II) is displayed in Fig. 5b. The four peaks corresponding to the anodic stripping of $Zn^{2+}$, $Cd^{2+}$, $Pb^{2+}$ and $Cu^{2+}$ are well resolved and the separation between the stripping peaks is well enough. It shows the potential applications of the HCS-188-44 in the simultaneous determination of coexisting heavy metal ions. In this case, the stripping peak currents of Cd(II) and Pb(II) are significantly higher than those of Zn(II) and Cu(II). Meanwhile, the stripping peak current (10.3 μA) of 83 nM Pb(II) in the pres-

Table 2 Electrochemical performance of various electrodes

| Electrode | Sensitivity (μA $μM^{-1}$) | Detection limit (nM) | Ref. |
|---|---|---|---|
| Nitrogen-doped microporous carbon | 1.9 | 0.61 | 7 |
| Graphene modified carbon nanosheet | 92.9 | 1.12 | 11 |
| $SnO_2$/reduced graphene oxide | 18.6 | 0.18 | 13 |
| γ-AlOOH@$SiO_2$/$Fe_3O_4$ | 81.5 | 0.01 | 28 |
| Porous $Co_3O_4$ microsheets | 71.6 | 18.00 | 29 |
| Nanosized hydroxyapatite/ionophore | 13.0 | 1.00 | 30 |
| Hollow carbon nanospheres | 160.0 | 0.60 | This work |

ence of Zn(II), Cd(II), and Cu(II) is a little lower compared with individual analysis (13.1 μA).

## Conclusions

In summary, our study provides a fundamental understanding of the structure–activity relationship of the electrodes by constructing a nano-patterned carbon electrode as a model system. There exists a "golden size" of HCSs, with which the electrochemical system exhibits the maximum sensitivity and minimum electron-transfer resistance. This study provides a new approach to push the sensing performance limit forward through the ingenuity that goes into an ordered electrode architecture.

## Experimental section

### PS@PF nanospheres

According to the method described previously, firstly, monodisperse PS with a specific particle size (~200, 280 nm) was prepared through emulsion polymerization; secondly, 150 mg PS were dispersed in 100 mL water, then a 20 mL volume of aqueous solution containing phenol and hexamethylenetetramine was added (Table S2†). After stirring gently for about 30 min, the solution was transferred into a Teflon-lined autoclave and heated at 160 °C for 4 h. The product was denoted as PS@PF.

### PS@PF@mSiO$_2$ nanospheres

0.48 g cetyltrimethyl-ammonium bromide (CTAB) was stirred with 15 mL water at 60 °C for 1 h. This solution was added to a mixture of 120 mg of PS@PF, 75 mL water, 30 mL ethanol, and 1.2 mL ammonia solution (28 wt%). The solution was stirred for 30 min before adding 0.84 mL of tetraethyl orthosilicate. The reaction was carried out at 30 °C for 16 h. PS@PF@SiO$_2$ was retrieved by centrifugation and allowed to react with an HCl alcohol solution (pH ~2) at 60 °C to remove CTAB from the silica shell. The final washed and dried product was denoted as PS@PF@mSiO$_2$.

### Synthesis of hollow carbon nanospheres

The as-made silica coating samples were heated at 3 °C min$^{-1}$ from room temperature to 150 °C and held at this temperature for 1 h under a nitrogen flow. The temperature was then ramped at 5 °C min$^{-1}$ to 600 °C and held at this temperature for 4 h. The pyrolyzed product was treated with aqueous NaOH solution (2.5 M) to remove silica, thus generating HCSs.

### Electrode preparation and electrochemical measurements

The construction of a HCS film on the surface of a GCE was performed as follows: 5 mg sample was suspended in 1 mL ethanol to form a suspension. The suspension was then briefly sonicated for 30 s in order to disperse the nanospheres. A 5 μL aliquot of this suspension was then pipetted onto the surface of a freshly polished glassy carbon electrode. And then a drop of the Nafion solution (0.5 wt%) was placed on the electrode surface and the solvents were left to evaporate at room temperature. All electrochemical measurements were performed using a CHI 660D (Shanghai CH Instruments, China) electrochemical workstation. Square wave anodic stripping voltammetry (SWASV) was used for the observation of electrochemical behavior under optimized conditions. Pb(II) was deposited at the potential of −1.0 V for 400 s by the reduction of Pb(II) in 1 M NaAc–HAc solution (pH = 5.5). The anodic stripping (re-oxidation of metal to metal ions) of the electrodeposited metal was performed in the potential range of −0.9 to −0.3 V with the following parameters: frequency, 15 Hz; amplitude, 25 mV; increment potential, 4 mV. The sample metal deposited on the electrode surface was removed by electrolysis at 0.3 V for 300 s in a fresh supporting electrolyte prior to the next cycle. EIS (electrochemical impedance spectra) were acquired in a solution containing 5 mM $Fe(CN)_6^{3-}/^{4-}$and 0.1 M KCl, and measured at an open circuit potential to Ag|AgCl|NaCl (3.0 M) and an alternating potential with an amplitude of 5 mV at the frequency range from 0.1 Hz to 10 000 Hz.

### Characterization

Scanning electron microscopy (SEM) investigations were carried out with a Hitachi S-4800 instrument. Transmission electron microscopy (TEM) analyses were carried out with a FEI Tecnai G$^2$20S-Twin equipment operating at 200 kV. The samples for TEM analysis were prepared by dropping an ethanol droplet of the products on carbon-coated copper grids and drying at room temperature.

## Acknowledgements

The project was supported by the National Program on Key Basic Research Project (no. 2013CB934104) and the National Natural Science Foundation of China (no. 21225312, 21473021 and U1303192).

## References

1 I. Ali, *Chem. Rev.*, 2012, **112**, 5073.
2 G. Aragay, J. Pons and A. Merkoçi, *Chem. Rev.*, 2011, **111**, 3433.
3 S. Mao, J. B. Chang, G. H. Zhou and J. H. Chen, *Small*, 2015, **11**, 5336.
4 H. G. Zhang, X. D. Yu and P. V. Braun, *Nat. Nanotechnol.*, 2011, **6**, 277.
5 Z. L. Li, J. Chen, J. Yang, Y. J. Su, X. Fan, Y. Wu, C. W. Yu and Z. L. Wang, *Energy Environ. Sci.*, 2015, **8**, 887.
6 L. S. Zhang, W. Li, Z. M. Cui and W. G. Song, *J. Phys. Chem. C*, 2009, **113**, 20594.
7 L. L. Xiao, H. B. Xu, S. H. Zhou, T. Song, H. H. Wang, S. Z. Li, W. Gan and Q. H. Yuan, *Electrochim. Acta*, 2014, **143**, 143.

8 G. Aragay, J. Pons and A. J. Merkoçi, *J. Mater. Chem.*, 2011, **21**, 4326.
9 A. Afkhami, H. Bagheri, H. Khoshsafara, M. Saber-Tehrani, M. Tabatabaeed and A. Shirzadmehr, *Anal. Chim. Acta*, 2012, **746**, 98.
10 S. Su, W. H. Wu, J. M. Gao, J. X. Lu and C. H. Fan, *J. Mater. Chem.*, 2012, **22**, 18101.
11 J. T. Zhang, Z. Y. Jin, W. C. Li, W. Dong and A. H. Lu, *J. Mater. Chem. A*, 2013, **1**, 13139.
12 R. Seenivasan, W. J. Chang and S. Gunasekaran, *ACS Appl. Mater. Interfaces*, 2015, **7**, 15935.
13 Y. Wei, C. Gao, F. L. Meng, H. H. Li, L. Wang, J. H. Liu and X. J. Huang, *J. Phys. Chem. C*, 2012, **116**, 1034.
14 B. Wang, B. Luo, M. H. Liang, A. Wang, J. Wang, Y. Fang, Y. H. Chang and L. J. Zhi, *Nanoscale*, 2011, **3**, 5059.
15 G. K. Mor, K. Shankar, M. Paulose, O. K. Varghese and C. A. Grimes, *Nano Lett.*, 2006, **6**, 215.
16 O. K. Varghese, M. Paulose, K. Shankar, G. K. Mor and C. A. Grimes, *J. Nanosci. Nanotechnol.*, 2005, **5**, 1158.
17 C. A. Grimes, *J. Mater. Chem.*, 2007, **17**, 1451.
18 R. Zhang, L. Lin, Q. S. Jing, W. Z. Wu, Y. Zhang, Z. X. Jiao, L. Yan, R. P. Hanc and Z. L. Wang, *Energy Environ. Sci.*, 2012, **5**, 8528.
19 R. Raccis, A. Nikoubashman, M. Retsch, U. Jonas, K. Koynov, H. J. Butt, C. N. Likos and G. Fytas, *ACS Nano*, 2011, **5**, 4607.
20 Y. C. Jiao, D. D. Han, Y. Ding, X. F. Zhang, G. N. Guo, J. H. Hu, D. Yang and A. G. Dong, *Nat. Commun.*, 2015, **6**, 6420.
21 J. Wei, H. Wang, Y. H. Deng, Z. K. Sun, L. Shi, B. Tu, M. Luqman and D. Y. Zhao, *J. Am. Chem. Soc.*, 2011, **133**, 20369.
22 P. Y. Wang, C. W. Shields, T. H. Zhao, H. Jami, G. P. López and P. Kingshott, *Small*, 2016, **12**, 1309.
23 A. H. Lu, T. Sun, W. C. Li, Q. Sun, F. Han, D. H. Liu and Y. Guo, *Angew. Chem., Int. Ed.*, 2011, **50**, 11765.
24 S. Wang, W. C. Li, G. P. Hao, Y. Hao, Q. Sun, X. Q. Zhang and A. H. Lu, *J. Am. Chem. Soc.*, 2011, **133**, 15304.
25 C. M. Ruan, L. J. Yang and Y. B. Li, *Anal. Chem.*, 2002, **74**, 4814.
26 M. Basu, Z. W. Zhang, C. J. Chen, P. T. Chen, K. C. Yang, C. G. Ma, C. C. Lin, S. F. Hu and R. S. Liu, *Angew. Chem., Int. Ed.*, 2015, **54**, 6211.
27 E. S. Kim, N. Nishimura, G. Magesh, J. Y. Kim, J. W. Jang, H. Jun, J. Kubota, K. Domen and J. S. Lee, *J. Am. Chem. Soc.*, 2013, **135**, 5375.
28 Y. Wei, R. Yang, Y. X. Zhang, L. Wang, J. H. Liu and X. J. Huang, *Chem. Commun.*, 2011, **47**, 11062.
29 Z. G. Liu, X. Chen, J. H. Liu and X. J. Huang, *Electron. Commun.*, 2013, **30**, 59.
30 D. Pan, Y. Wang, Z. Chen, T. Lou and W. Qin, *Anal. Chem.*, 2009, **81**, 5088.

 